Upper bounds of spin-density wave energies in the homogeneous electron gas

F. Delyon,[1] B. Bernu,[1] L. Baguet,[1] and M. Holzmann[1,2]

[1]*Laboratoire de Physique Théorique de la Matière Condensée, UPMC, CNRS UMR 7600,*
Sorbonne Universités, 75252 Paris Cedex 05, France
[2]*LPMMC, UMR 5493 of CNRS, Université J. Fourier, BP 166, F-38042 Grenoble Cedex, France*

Studying the jellium model in the Hartree-Fock approximation, Overhauser has shown that spin-density waves (SDWs) can lower the energy of the Fermi gas, but it is still unknown whether these SDWs are actually relevant for the phase diagram. In this paper, we give a more complete description of SDW states. We show that a modification of the Overhauser ansatz explains the behavior of the jellium at high density compatibly with previous Hartree-Fock simulations.

PACS number(s): 71.10.Ca, 71.10.Hf, 71.30.+h

I. INTRODUCTION

The simplest model of electronic structure is jellium—electrons embedded in a homogeneous background of opposite charge such that the system is neutral. This model is a good starting point to describe properties of simple metals such as sodium [1]. At zero temperature, the only parameter of this model is the density n, or the dimensionless parameter $r_s = 3/(4\pi n a_B^3)^{1/3}$, where $a_B = \hbar^2/(me^2)$ is the Bohr radius. Within the Hartree-Fock approximation (HF), Overhauser has shown that the Fermi gas is unstable under a spin-density wave (SDW) [2,3]. Only recently, almost 50 years after Overhauser's prediction, explicit numerical estimates of the HF ground state have shown SDW evidence of the electron gas in three [4–7] and two dimensions [7,8]. Still, a quantitative estimate of the variation of the SDW amplitude and energy in the high-density region $r_s \lesssim 1$ is missing [9]. In this paper, we generalize Overhauser's ansatz and provide a quantitative solution of this long-standing problem.

Beyond Hartree-Fock, the relevance of SDWs in the phase diagram of the electron gas remains unclear due to the competition with correlations [10,11]. However, up-to-date, all-numerical methods used for quantitative computation of correlation effects [12–14] elaborate on a certain reference ground state—in general taken from a Hartree-Fock or density functional based wave function. Although the resulting (approximate) ground state wave function of the finite system incorporates strong many-body correlations, the underlying structure of the reference function most likely remains unchanged [15]. We hope that the detailed understanding of SDWs in HF with quantitative energy bounds will also contribute to clarify the role of correlation on this phase.

The key point of a quantitative understanding of SDWs in HF is to search for a solution in a nonperturbative way. Indeed, small domains exist around the Fermi surface where the one-body states differ radically from a single plane wave. These states of wave vector $\mathbf{k}$ are coupled with the wave vector $\mathbf{k} + \mathbf{Q_k}$ where $\mathbf{Q_k}$ is constant over each domain. The larger is this domain, the larger will be the energy gain of the SDWs. One way to enlarge this domain is to cut the top of the sphere as explained by Overhauser [2]. In the following we show that adding a small cylinder on the top of the truncated sphere as shown in Fig. 1 can increase the energy gain of

the SDW by orders of magnitude compared to Overhauser's ansatz. Furthermore, we provide an explicit estimate of the energy gain of the SDW state. As we will see, the optimal size of these domains dramatically shrinks with increasing density, resulting in an extremely rapid decrease of the tiny SDW energy gain and explaining the difficulties of observing SDWs in the high-density region.

Our semianalytical results presented here are compared to recent HF results [6] obtained with periodic models. Indeed, Overhauser's ansatz is in fact a periodic model (a crystal where the one-body states are limited to the first mode) as soon as the set vectors $\mathbf{Q_k}$ belong to a discrete lattice. As the density increases the number of vectors $\mathbf{Q_k}$ (and of domains around the Fermi sphere) may also increases [2] leading to a quasicrystal which cannot be described by a periodic model.

Let us mention that in this paper we focus on the SDW states. These states are easier to compute leading to simpler formulas since the density of charge is constant. Equivalent results may be obtained [2,3] for the charge-density waves (CDWs).

In the following, we outline the main steps in the calculation of the SDW energies. First we introduce the deformation of the Fermi surface generalizing Overhauser's model and describe the SDW ansatz for the single-particle states. We then show how the optimal solution can be found by calculating the fixed point solution of a nonlinear functional equation. The explicit results are then obtained by restricting ourselves to a one-dimensional function and comparing to the outcome of previous numerical simulations.

II. FERMI GAS ENERGY OF THE TRUNCATED SPHERE

Let us call E_{FG} the HF energy of the Fermi gas where only plane wave states of wave vectors $\mathbf{k}$ inside the Fermi sphere of radius k_F are occupied. Following Overhauser, in a first step the Fermi sphere is deformed into a volume $\mathcal{F}$ as shown in Fig. 1, and its energy increase is denoted $\Delta E_{\text{FG}}^{\mathcal{F}} = E_{\text{FG}}^{\mathcal{F}} - E_{\text{FG}}$. Here, the subscript FG is used to point out that the many-body state is a Slater determinant of plane wave states inside the corresponding Fermi surface. Using k_F as unit of wave vectors, the sphere in Fig. 1 has unit radius, and the deformation is characterized by a small parameter ϵ approaching zero as r_s decreases. In order to keep the electron density constant, the

FIG. 1. Shape of occupied zones for spiral SDWs. $\mathcal{F}_\uparrow$ (plain line) and $\mathcal{F}_\downarrow$ (dashed line) are built from truncated sphere plus a small cylinder. A perturbed spin-up state is a superposition of a spin-up plane wave $e^{i\mathbf{k}\mathbf{r}}$ on a spin-down plane wave $e^{i(\mathbf{k}+\mathbf{Q_k})\mathbf{r}}$ with $Q = \|\mathbf{Q_k}\| = 2(1 - \epsilon + h\epsilon)$.

deformed surface in Fig. 1 must be scaled by R such that $R^3 \int_{\mathcal{F}_\uparrow} d\mathbf{k} = R^3 \int_{\mathcal{F}_\downarrow} d\mathbf{k} = 4\pi/3$ (see Ref. [16]). The Fermi gas energy per particle in Hartree units [$Ha = \hbar^2/(ma_B^2)$] is

$$E_{\mathrm{FG}}^{\mathcal{F}} = \frac{a_K R^5}{r_s^2} K_{\mathrm{FG}} - \frac{a_V R^4}{r_s} V_{\mathrm{FG}}, \quad (1)$$

$$K_{\mathrm{FG}} = \int_{\mathcal{F}_\uparrow + \mathcal{F}_\downarrow} d\mathbf{k}\, k^2, \quad (2)$$

$$V_{\mathrm{FG}} = \int_{\mathcal{F}_\uparrow \times \mathcal{F}_\uparrow + \mathcal{F}_\downarrow \times \mathcal{F}_\downarrow} d\mathbf{k}\, d\mathbf{k}' \frac{1}{|\mathbf{k} - \mathbf{k}'|^2}, \quad (3)$$

with $a_V = \frac{3}{32\pi^3}(\frac{9\pi}{4})^{1/3}$, $a_K/a_V = 2\pi^2(\frac{9\pi}{4})^{1/3} \approx 37.9$.

The energy change, $\Delta E_{\mathrm{FG}}^{\mathcal{F}}$, can be computed by direct integration (see Fig. 2) and gives at the leading order in ϵ (see Ref. [17])

$$\Delta E_{\mathrm{FG}}^{\mathcal{F}} \approx \frac{2\pi^2 a_V \epsilon^3}{r_s}\left[\alpha(\gamma - 1) - \frac{1}{9} + h\right] \quad (4)$$

with $\alpha = 2(h - \frac{1}{2})^2 + \frac{1}{6}$ and $\gamma = \ln\frac{2}{\epsilon} + \frac{a_K}{a_V \pi r_s}$. For small r_s, ϵ is small and thus γ is large. The minimum of $\Delta E_{\mathrm{FG}}^{\mathcal{F}}$ with

FIG. 2. (Color online) $\Delta E_{\mathrm{FG}}^{\mathcal{F}}$ as a function of h for different values of ϵ at $r_s = 4$.

respect to h is for $h = \frac{1}{2} - \frac{1}{4(\gamma - 1)} \approx \frac{1}{2}$, and, for small r_s, $\Delta E_{\mathrm{FG}}^{\mathcal{F}}$ is four times smaller than in the Overhauser case ($h = 0$).

III. ENERGY OF THE SPIN-DENSITY WAVES

In a second step, the SDWs are obtained by replacing a plane wave $|\mathbf{k}, \uparrow\rangle$ by $a_\mathbf{k}|\mathbf{k}, \uparrow\rangle + b_\mathbf{k}|\mathbf{k} + \mathbf{Q_k}, \downarrow\rangle$ ($|a_\mathbf{k}|^2 + |b_\mathbf{k}|^2 = 1$), for $\mathbf{k}$ in $\mathcal{F}_\uparrow$. Symmetrically, for $\mathbf{k}$ in $\mathcal{F}_\downarrow$, a plane wave $|\mathbf{k}, \downarrow\rangle$ is replaced by the combination $a'_\mathbf{k}|\mathbf{k}, \downarrow\rangle + b'_\mathbf{k}|\mathbf{k} + \mathbf{Q_k}, \uparrow\rangle$ with $a'_\mathbf{k} = a_{-\mathbf{k}}$ and $b'_\mathbf{k} = b_{-\mathbf{k}}$. We choose $a_\mathbf{k}$ real and positive and in the following we assume that $b_\mathbf{k}$'s are also positive and that $b_\mathbf{k} < a_\mathbf{k}$ [18].

As in Fig. 1, $\mathbf{Q_k}$ is such that for $\mathbf{k}$ in $\mathcal{F}_\uparrow$, $\mathbf{k} + \mathbf{Q_k}$ does not belong to $\mathcal{F}_\downarrow$, and for $\mathbf{k}$ in $\mathcal{F}_\downarrow$, $\mathbf{k} + \mathbf{Q_k}$ does not belong to $\mathcal{F}_\uparrow$. The energy change is given by

$$\Delta E_{\mathrm{SDW}}^{\mathcal{F}} = \frac{2a_K R^5}{r_s^2} K_{\mathrm{SDW}} - \frac{2a_V R^4}{r_s} V_{\mathrm{SDW}}, \quad (5)$$

$$K_{\mathrm{SDW}} = \int_{\mathcal{F}_\uparrow} d\mathbf{k}\, (\|\mathbf{k} + \mathbf{Q_k}\|^2 - k^2)b_\mathbf{k}^2, \quad (6)$$

$$V_{\mathrm{SDW}} = -\int_{\mathcal{F}_\uparrow \times \mathcal{F}_\uparrow} d\mathbf{k} d\mathbf{k}'\, \frac{(a_\mathbf{k} b_{\mathbf{k}'} - b_\mathbf{k} a_{\mathbf{k}'})^2}{\|\mathbf{k} - \mathbf{k}'\|^2}$$

$$+ \int_{\mathcal{F}_\uparrow \times \mathcal{F}_\uparrow} d\mathbf{k} d\mathbf{k}'\, \frac{(a_\mathbf{k} b_{\mathbf{k}'} + b_\mathbf{k} a_{\mathbf{k}'})^2}{\|\widetilde{\mathbf{k}} - \mathbf{k}'\|^2}, \quad (7)$$

with $\widetilde{k}_z = Q - k_z$ (see Fig. 1). Using the linear symmetric operators $T^\pm$:

$$(T^\pm f)(\mathbf{k}) = \int_{\mathcal{F}_\uparrow} d\mathbf{k}'\left(\frac{1}{\|\mathbf{k} - \mathbf{k}'\|^2} \pm \frac{1}{\|\widetilde{\mathbf{k}} - \mathbf{k}'\|^2}\right)f(\mathbf{k}'), \quad (8)$$

Eq. (5) can be rewritten

$$\Delta E_{\mathrm{SDW}}^{\mathcal{F}} = \frac{4a_V R^4}{r_s}[2(\kappa, b^2) + (T^- a^2, b^2) - (T^+ ab, ab)], \quad (9)$$

where (f, g) is the scalar product $\int_{\mathcal{F}_\uparrow} fg$, and $2\kappa(k) = \frac{a_K R}{2a_V r_s} Q(Q - 2k_z) \geqslant 0$. In Eq. (9) the difference between 1 and R is negligible and in the following we set $R = 1$.

A. Optimal solution

From the variations of Eq. (9) with respect to $b_\mathbf{k}$, the optimal function b satisfies

$$2b\kappa + bT^-(a^2 - b^2) = \frac{a^2 - b^2}{a}T^+ab. \quad (10)$$

Setting $\xi = ab$ and using $b^2 \leqslant \frac{1}{2}$, $a^2 - b^2 = \sqrt{1 - 4\xi^2}$, Eq. (10) can be rewritten $\xi = J(\xi)$, where

$$J(\xi) = \frac{1}{2}\frac{T^+ \xi}{\sqrt{(\kappa + T^- \sqrt{1/4 - \xi^2})^2 + (T^+ \xi)^2}}. \quad (11)$$

Thus the point is now to find the fixed points of the operator J. The Fermi gas ($\xi = 0$) is a trivial fixed point. By definition $0 \leqslant \xi \leqslant \frac{1}{2}$, and from Eq. (11), we see that $0 \leqslant J(\xi) \leqslant \frac{1}{2}$. We claim that starting with $\xi = 1/2$ and iterating the process

$\xi \to J(\xi)$ leads to a nontrivial fixed point satisfying

$$\xi(k_z = Q/2) = \tfrac{1}{2}. \tag{12}$$

Indeed, by Eq. (8) the kernels of $T^\pm$ are positive, and thus $T^\pm$ are positivity-preserving linear operators: if $\xi \geqslant \xi'$, then $T^+\xi \geqslant T^+\xi'$; similarly $T^-\sqrt{1/4 - \xi^2} < T^-\sqrt{1/4 - \xi'^2}$, and consequently,

$$\xi \geqslant \xi' \Rightarrow J(\xi) \geqslant J(\xi'). \tag{13}$$

Thus starting with $\xi_0 = 1/2$, we have $J(\xi_0) \leqslant \xi_0$ and setting $\xi_n = J(\xi_{n-1})$, ξ_n is a decreasing sequence of positive functions and thus converges to a fixed point ξ_∞.

B. 1-D approximation

Now we impose that $b_\mathbf{k}$ (thus $\xi_\mathbf{k}$) is nonzero only in the cylinder $\mathcal{C}$ corresponding to the gray region of Fig. 1 where it depends only on k_z: $\mathcal{C} = \{\mathbf{k} : k_x^2 + k_y^2 \leqslant r^2 = 1 - (1 - \epsilon)^2 \approx 2\epsilon, 0 \leqslant k_z \leqslant Q\}$. As we shall see below, $b_\mathbf{k}$ differs from zero only in the neighborhood of the top disk of $\mathcal{F}_\uparrow$ (and its symmetric for $\mathcal{F}_\downarrow$). In any case, these restrictions always provide an upper bound for the energy of the SDW.

First, for the second term of Eq. (9), we have

$$(a^2, T^-b^2) = (b^2, T^-a^2) = (b^2, T^-1) - (b^2, T^-b^2). \tag{14}$$

From Eq. (8), $T^-1 = v_\mathcal{F}(\mathbf{k}) - v_\mathcal{F}(\widetilde{\mathbf{k}})$, where $v_\mathcal{F}$ is the potential induced by the truncated sphere. In the spherical case, the potential of the unit sphere is given by

$$v(\mathbf{k}) = 2\pi + \pi \frac{1 - k^2}{k} \ln \frac{1 + k}{|1 - k|}.$$

In this case, for k close to 1 ($\mathbf{k}$ and $\widetilde{\mathbf{k}}$ are close and near the unit sphere and $\widetilde{k}_z = 2 - k_z$), $v(\mathbf{k}) - v(\widetilde{\mathbf{k}}) \approx -4\pi(1 - k)\ln(\frac{1-k}{2})$. This singular behavior is associated with the discontinuity of the density (in $\mathbf{k}$ space). An analytic solution is provided for the truncated sphere [17]. This solution has the same behavior except that $1 - k$ has to be replaced by the distance of $\mathbf{k}$ to the discontinuity of the density, i.e., the top disk of $\mathcal{F}_\uparrow$:

$$(T^-1)(\mathbf{k}) \approx -4\pi(Q/2 - k_z) \ln\left(\frac{|Q/2 - k_z|}{2}\right), \tag{15}$$

provided that $|Q/2 - k_z| \ll 1$. For $h > 0$, Eq. (15) is still valid [17] except in a small neighborhood of the edge of the top disk. In the following we neglect this effect and apply Eq. (15) also for $h > 0$.

Using the scaled distance $x = (Q/2 - k_z)/r$,

$$2\kappa + T^-1 = 2\pi r[\gamma x - 2x \ln(x)], \tag{16}$$

and integrating over $\mathbf{q} = (k_x, k_y)$, Eq. (9) becomes

$$\Delta E_{\text{SDW}}^\mathcal{F} = \frac{4\pi a_V r^4}{r_s} \delta E_{\text{SDW}}^\mathcal{F}, \tag{17}$$

$$\delta E_{\text{SDW}}^\mathcal{F} = 2\pi(\gamma x - 2x \ln(x), b^2) - (T^-b^2, b^2) - (T^+\xi, \xi), \tag{18}$$
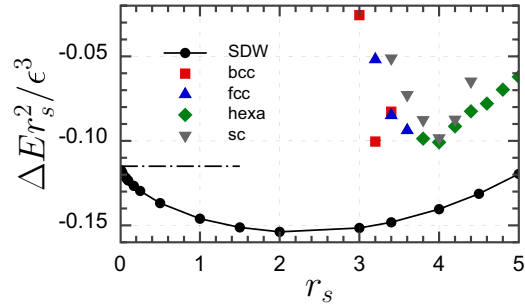
FIG. 3. (Color online) Renormalized energy $\Delta E r_s^2/\epsilon^3$ as a function of the density. The dashed-dotted line stands for the analytical solution: $\Delta E r_s^2/\epsilon^3 = -0.115$. The black circles stand for the SDW simulations. Other symbols stand for HF energies (see Fig. 5 of Ref. [6]).

where the scalar product is now $(f, g) = \int_{x>0} dx\, f(x)g(x)$, and $T^\pm$ become in terms of x

$$(T^\pm f)(x) = \pi \int_0^{1/r} dx'[G(x - x') \pm G(x + x')]f(x'), \tag{19}$$

$$G(x) = \frac{1}{\pi^2 r^2} \int_{q^2, q'^2 < r^2} d\mathbf{q}\, d\mathbf{q}' \frac{1}{r^2 x^2 + (\mathbf{q} - \mathbf{q}')^2} \tag{20}$$

$$= 2\ln\left[1 + \frac{2}{|x|u}\right] - \frac{4}{u^2}, \quad u = |x| + \sqrt{x^2 + 4}. \tag{21}$$

In fact, for small r_s, the term (T^-b^2, b^2) may be neglected in Eq. (18) [17]. In any case, since T^- is a positive operator, we get an upper bound for the energy and the variation of the resulting upper bound leads to $\xi = J\xi$, where J is now an operator on the positive functions on $\mathbb{R}^+$:

$$J(\xi) = \frac{1}{2} \frac{T^+\xi}{\sqrt{\pi^2[\gamma x - 2x \ln(x)]^2 + (T^+\xi)^2}}. \tag{22}$$

As above, the fixed point of Eq. (22) can be easily found by iteration.

Thereafter, for fixed r_s the total energy variation $\Delta E(\epsilon, h) = \Delta E_{\text{FG}}^\mathcal{F}(\epsilon, h) + \Delta E_{\text{SDW}}^\mathcal{F}(\epsilon)$ is computed and optimized with respect to ϵ. For $r_s = 3$ about 20 iterations of the operator J are required and about 100 iterations for $r_s = 0.01$ (see black circles in Fig. 3).

In the next paragraph, we give a solution for ξ at small r_s and deduce the scaling of ΔE from it.

C. Analytic solution for small r_s

For small r_s, γ is large and Eq. (22) can be solved approximately [17]:

$$\xi(x) \approx \frac{1}{2\sqrt{\frac{x^2}{x_0^2} + 1}} \cos\left[\sqrt{\frac{2}{\gamma'}} \operatorname{arcsinh}\left(\frac{x}{x_0}\right)\right], \tag{23}$$

$$x_0 = 2\exp\left(-\frac{\pi}{2\sqrt{2}}\sqrt{\gamma'} - \frac{1}{2}\right), \tag{24}$$

for $2\pi\sqrt{2}(\gamma'-\gamma)=\sqrt{\gamma}(\pi^2+4)$, leading to the asymptotic behavior of $\Delta E_{\mathrm{SDW}}^{\mathcal{F}}$:

$$\Delta E_{\mathrm{SDW}}^{\mathcal{F}}(\epsilon)\lesssim -C\frac{2\pi^2 a_V}{r_s}\epsilon^2\gamma\exp\left(-\frac{\pi}{\sqrt{2}}\sqrt{\gamma}\right),\quad (25)$$

with $C=8e^{-3/2-\pi^2/8}$.

IV. EVALUATION OF THE BEST TOTAL ENERGY

Now Eqs. (4) and (25) provide the behavior of $\Delta E(\epsilon,h)$:

$$\begin{aligned}\Delta E &= \Delta E_{\mathrm{SDW}}^{\mathcal{F}} + \Delta E_{\mathrm{FG}}^{\mathcal{F}}\\ &= \frac{2\pi^2 a_V \gamma \epsilon^2}{r_s}\left[\epsilon\alpha - C\exp\left(-\frac{\pi}{\sqrt{2}}\sqrt{\gamma}\right)\right].\end{aligned}\quad (26)$$

The minimum energy is at $\epsilon=\epsilon_0[1+O(\sqrt{r_s})]$:

$$\Delta E \approx -\frac{\pi a_K \alpha}{r_s^2}\epsilon^3,\quad (27)$$

$$\epsilon_0 = \frac{2C}{3\alpha}e^{-\pi^2/4-\pi\sqrt{\gamma_0/2}} \approx \frac{0.0294 e^{-7.714/\sqrt{r_s}}}{\alpha},\quad (28)$$

where $\gamma_0 = a_K/(a_V\pi r_s)$. Equation (27) shows that at small r_s, $\Delta E\, r_s^2/\epsilon^3$ goes to a constant. Figure 3 shows the numerical results for the scaled energy at $h=1/2$ (black circles). This scaled energy is of order -0.1 over a wide range of r_s. On the other hand, while ϵ_0, Eq. (28), varies over decades when r_s decreases, Fig. 4 shows that the ratio ϵ/ϵ_0 is a slowly varying function. The analytical result is supposed to be relevant for large γ, that is, for $\frac{3}{\sqrt{r_s}}\gg 1$. This can be verified in the figure: the next corrections in Eqs. (27) and (28) behave as $\sqrt{r_s}$.

A. Influence of h

The dependency in h is through the parameter α; see Eq. (4). Figure 5 shows the effect of h on ϵ and ΔE obtained numerically. For small r_s, at $h=1/2$ (thus $\alpha=1/6$), the energy is actually 16 times larger than in the Overhauser model ($h=0$, $\alpha=2/3$). At larger r_s, this ratio can be significantly increased; e.g., it is about 200 for $r_s=5$. In this region we expect the energy gain to deeply rely on the precise shape of $\mathcal{F}$.
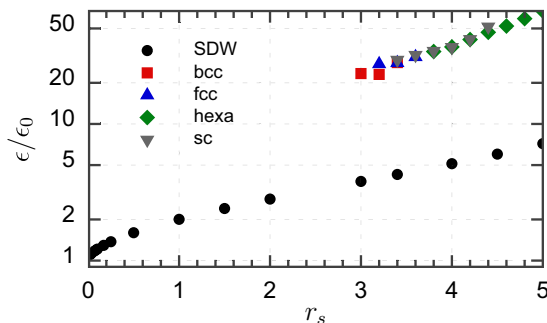
FIG. 4. (Color online) Scaled parameter ϵ/ϵ_0 as a function of the density. ϵ_0 is the value of Eq. (28) for $h=1/2$. The black circles stand for the present work, while other symbols stand for HF results [6].
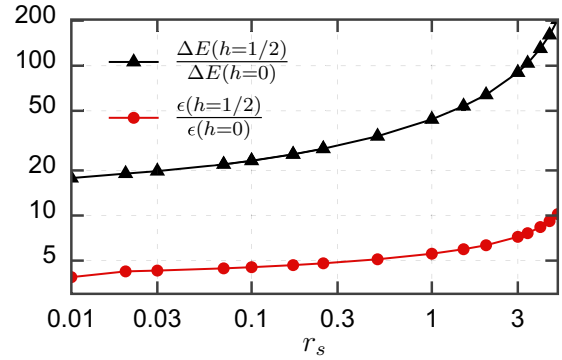
FIG. 5. (Color online) Influence of h on the energy gain versus r_s: the triangles represent the energy and the circles the ϵ ratios.

B. Comparison with HF simulations

In previous HF computations of the jellium [6,7] we have considered a discretized Fermi sphere of 64^3, 96^3, and 128^3 values of **k**. This corresponds to 32, 48, and 64 equally distributed values of k in the interval $(0,1)$. For $r_s < 5$ evidence of SDW ground states has been found [6]. In Figs. 3 and 4, we show the corresponding energy gain per number of SDWs (2 for hexa up to 12 for bcc). The larger energy gain of the HF simulations for $r_s \geqslant 3$ can be mostly attributed to a smoother and better optimized shape, compared to the simple cylinder used in the analytical SDW; other assumptions such as the 1-dimensional approximation decrease the energy further by a factor of 2–3. For $r_s < 3$, the discretization of the Fermi sphere becomes crucial, and even the simulations with 128^3 k points used in [6] are insufficient to resolve the expected SDW amplitudes leading to the standard Fermi gas ground state ($\epsilon = 0$ and $b_{\mathbf{k}} = 0$). Direct numerical simulations of the SDW in this high-density region will require a significant increase of k points by several order of magnitude.

V. CONCLUSION

Considering the ground state of jellium in the Hartree-Fock approximation, we quantified the energy of the SDW suggested by Overhauser. Furthermore, we prove that a modification of the truncated Fermi sphere leads to an energy gain 16 to 200 times larger than in the Overhauser model.

Our results readily extend to a polarized model: in Eq. (7) we have to take into account the direct potential which appears with a factor $1/Q^2$ and thus is negligible at small r_s (of order ϵ^4).

In order to obtain the energy of jellium, the results of Fig. 3 must be multiplied by the number of SDWs. For simple periodic models considered in previous works, this factor varies from 2 (hexa) up to 12 (bcc). At very small r_s, the perturbation of the SDW is localized in tiny regions which do not interact; thus, one may suppose that we can have many of them distributed around the Fermi sphere giving rise to a quasiperiodic behavior of the spin density.

The role of electronic correlations on the stability of SDWs beyond HF remains still open. Our calculations show that the energy gain in the high-density region, $r_s \lesssim 1$, where SDWs were searched for, is unexpectedly small and becomes

rapidly unobservable with increasing density. In addition, direct observation of SDWs in HF requires an extremely fine mesh of k points corresponding to very large systems. Typical system sizes used in post-HF calculations [12–14] are likely far too small to directly observe SDWs as, already in HF, extremely large sizes are needed for their occurrence.

[1] S. Huotari, J. A. Soininen, T. Pylkkänen, K. Hämäläinen, A. Issolah, A. Titov, J. McMinis, J. Kim, K. Esler, D. M. Ceperley, M. Holzmann, and V. Olevano, Phys. Rev. Lett. **105**, 086403 (2010).

[2] A. W. Overhauser, Phys. Rev. Lett. **4**, 462 (1960); Phys. Rev. **128**, 1437 (1962).

[3] G. F. Giuliani and G. Vignale, *Quantum Theory of the Electron Liquid* (Cambridge University Press, Cambridge, 2005).

[4] S. Zhang and D. M. Ceperley, Phys. Rev. Lett. **100**, 236404 (2008).

[5] F. G. Eich, S. Kurth, C. R. Proetto, S. Sharma, and E. K. U. Gross, Phys. Rev B **81**, 024430 (2010).

[6] L. Baguet, F. Delyon, B. Bernu, and M. Holzmann, Phys. Rev. Lett. **111**, 166402 (2013); Phys. Rev. B **90**, 165131 (2014).

[7] L. Baguet, Ph.D. thesis, Université Pierre et Marie Curie, 2014, https://tel.archives-ouvertes.fr/tel-01127918.

[8] B. Bernu, F. Delyon, M. Holzmann, and L. Baguet, Phys. Rev. B **84**, 115115 (2011).

[9] An estimate is missing apart from B. Bernu, F. Delyon, M. Duneau, and M. Holzmann, Phys. Rev. B **78**, 245110 (2008). But this estimate is overruled by the present work.

[10] D. R. Hamann and A. W. Overhauser, Phys. Rev. **143**, 183 (1966).

[11] A. W. Overhauser, Phys. Rev. **167**, 691 (1968).

[12] D. M. Ceperley and B. J. Alder, Phys. Rev. Lett. **45**, 566 (1980).

[13] J. J. Shepherd, G. Booth, A. Grüneis, and A. Alavi, Phys. Rev. B **85**, 081103(R) (2012).

[14] J. J. Shepherd, T. M. Henderson, and G. E. Scuseria, J. Chem. Phys. **140**, 124102 (2014).

[15] M. Taddei, M. Ruggeri, S. Moroni, and M. Holzmann, Phys. Rev. B **91**, 115106 (2015).

[16] For given ϵ and $0 \leqslant h \leqslant 1$, the radius of the truncated sphere satisfies $R^3[4 + 3\epsilon^2(1 - 2h) + \epsilon^3(1 - 3h)] = 4$.

[17] See Supplemental Material at http://link.aps.org/supplemental/10.1103/PhysRevB.92.235124 for a detailed derivation of the Fermi gas energies (file Supp-Energies.pdf), and how the 1D-SDW energy is obtained (file Supp-SDW.pdf).

[18] One easily checks afterwards that the optimal energy is obtained for $b_{\mathbf{k}}$'s with a constant arbitrary phase.